

# Volcaniclastic rocks and reconstruction of a volcanosedimentary paleoenvironment in Campos Basin, SE Brazil

Yara Veloso Magalhães Frank<sup>1\*</sup> , Sérgio de Castro Valente<sup>1</sup> 

## Abstract

Santonian-Campanian tuffaceous siltstone, epiclastic siltstone, arkose, and fossiliferous mudstone occur in a 45-m-thick section of well 1-BR-SA-37-RJS drilled in the southern Campos Basin, offshore SE Brazil. Well log data and petrographic and lithogeochemical data obtained from cutting samples were used to propose a schematic model of the volcano's sedimentary paleoenvironment. The volcaniclasts in the tuffaceous siltstone and epiclastic siltstone are scoria basalts, typical of spatter cones associated with monogenetic fields worldwide. The combination of these features with the petrographic ones of the arkoses found in the same well interval is likely to be related to volcaniclastic processes taking place on the continental shelf. Ratios between the immobile trace elements of the volcaniclastic rocks can be explained by mixing between sources in the upper continental crust adjacent to southern Campos and the scoria basalts extruded in the monogenetic fields. The little differentiated, olivine-rich basalts extruded from the scoria and spatter cones suggest a rising asthenosphere mantle extending from hundreds of kilometers eastwards till southern Campos in the Santonian-Campanian. This may have resulted in regional discordances in the Santonian, both in the Campos and Santos basins, and also places the petroleum systems in the southern Campos Basin under the thermal influence of such a rising asthenosphere in the Santonian-Campanian.

**KEYWORDS:** volcaniclastic rocks; Campos Basin; volcanosedimentary paleoenvironment; geochemistry; binary mixing.

## INTRODUCTION

Volcaniclastic processes are difficult to understand because fragmentation, transport, and depositional processes may be rather complex due to interactions between magmatic and sedimentary mechanisms, requiring an interdisciplinary approach (Manville *et al.* 2009). Complexities defy even classification proposals (Fisher 1961, Cas and Wright 1987, McPhie *et al.* 1993, Critelli and Ingersoll 1995, White and Houghton 2006, Di Capua and Gropelli 2018, Sohn and Sohn 2019, Di Capua *et al.* 2022), even though volcaniclasts can provide valuable information about processes occurring in continental and marine environments and for reconstructing the tectonic and palaeogeographical evolution of sedimentary basins and related volcanic and geodynamic settings (Dickinson 1985, Valloni 1985, Zuffa 1987, Ingersoll 1990, Garzanti *et al.* 2007, Critelli and Criniti 2021, Critelli *et al.* 2022).

The post-Aptian magmatism is widespread in the southern Campos and northern Santos basins and has peaks at the Santonian and Eocene (Caddah *et al.* 1994, 1998, Alves 2006, Moreira *et al.* 2006, Oreiro 2006, Oreiro

*et al.* 2008, Rangel 2006, Winter *et al.* 2007, Correia *et al.* 2019, Louback *et al.* 2021, Matos 2021, Mohriak *et al.* 2022). Volcaniclastic processes have been described in the Campos and Santos basins (Alves 2006, Moreira *et al.* 2006), but reconstructions of sedimentary paleoenvironments have been proposed for the Campos Basin, mostly on the basis of sequence stratigraphy and geophysical data (Alvarenga *et al.* 2021, Armelenti *et al.* 2021, Mohriak *et al.* 2021; Pandolpho *et al.* 2021). However, previous works have not discriminated against the volcanic setting of such volcanosedimentary paleoenvironments.

Works with volcaniclastic rocks elsewhere have demonstrated that combined petrographic and lithogeochemical data can be used to assess their provenance, which can be reasonably constrained based on trace element and isotope data (Graham *et al.* 1997, Gill *et al.* 2018). This article presents new petrophysical, petrographic, and lithogeochemical data for a Santonian-Campanian volcaniclastic section sampled by a well drilled in an area with prominent volcanism in the southern Campos Basin, SE Brazil. Petrophysical data were used to discriminate different log-facies that were further correlated with petrographic data, allowing the proposal of possible structures within volcaniclastic beds. The interpretation of the petrographic and lithogeochemical data combined with previously published geophysical data presented in this article may contribute to the understanding of volcaniclastic processes in general and the evolution of the Campos Basin.

<sup>1</sup>Department of Petrology and Geotectonics, Universidade Federal Rural do Rio de Janeiro – Seropédica (RJ), Brazil. E-mails: ymveloso@outlook.com, sergio@ufrj.br

\*Corresponding author.



## GEOLOGICAL SETTING

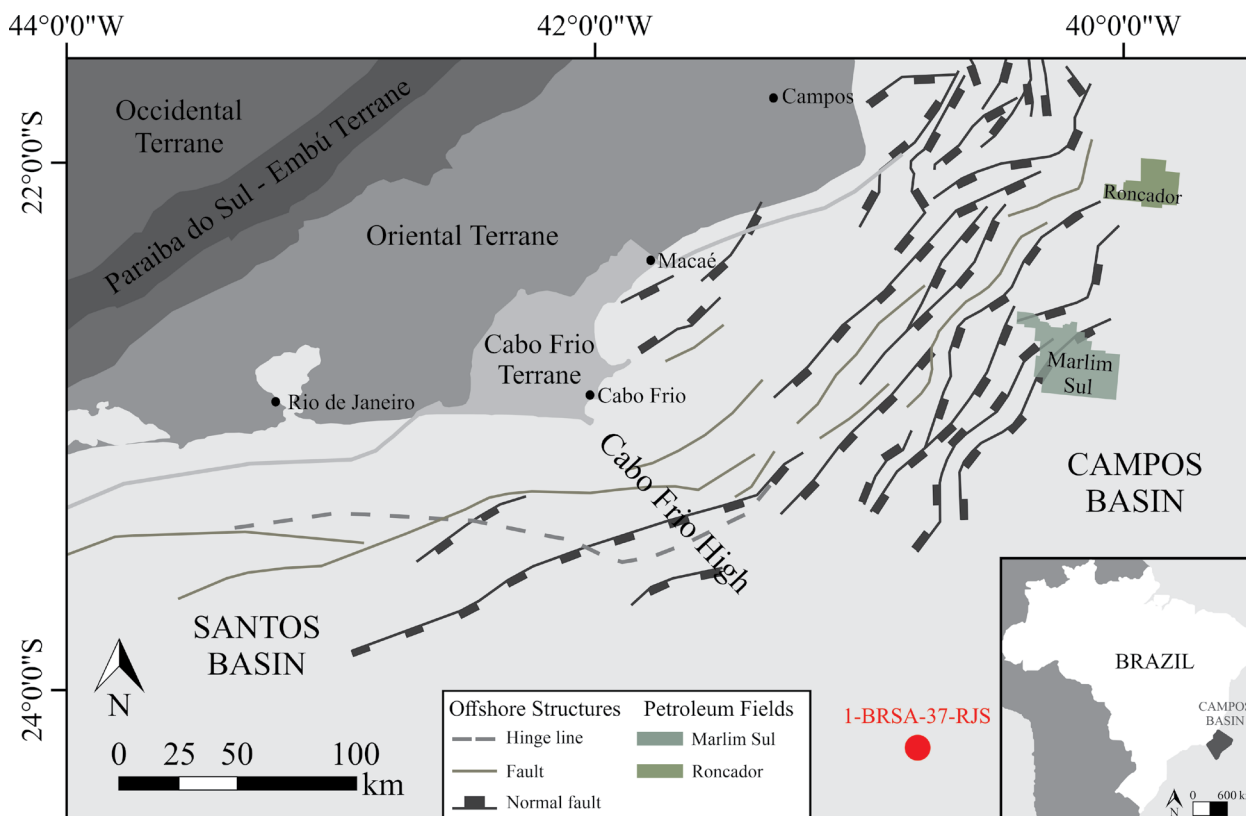
The Campos Basin is located on the continental margin of SE Brazil (Fig. 1) and covers an area of more than 100,000 km<sup>2</sup> (Dias *et al.* 1988). The borders of the basin are the Vitória Structural High, to the north, and the Cabo Frio Structural High, to the south, respectively, with the Espírito Santo and Santos basins. The igneous and metamorphic rocks of the Upper Proterozoic Ribeira and Araçuaí collisional orogens (*e.g.*, Heilbron *et al.* 2020, Caxito *et al.* 2022) constitute the western border and the crystalline basement of Campos Basin (Winter *et al.* 2007; Fig. 1).

The Campos Basin is a rift basin that evolved into an intraplate continental margin sedimentary basin because of the fragmentation of West Gondwana in the Lower Cretaceous and further opening of the South Atlantic Ocean (Chang *et al.* 1992). The largest oil reserves in Brazil were found in Campos Basin prior to the discovery of the giant pre-salt reservoirs in Santos Basin (Mello *et al.* 2021), both located offshore SE Brazil (Fig. 1). Still, Campos accounts for 22% of the oil production and 16% of the gas production in Brazil (ANP 2022). Magmatic processes may affect the petrophysical parameters of potential oil and gas reservoir sedimentary rocks (*e.g.*, Armelenti *et al.* 2021) and played a role during the sedimentation of the reservoir turbidites (Caddah *et al.* 1998, Fetter *et al.* 2009) in the major post-salt hydrocarbon fields in Campos, such as Roncador and Marlim Sul (Fig. 1), that produce more than 111,000 boe/d in Brazil (ANP 2022).

The chronostratigraphic chart of the basin (Winter *et al.* 2007) records magmatic events related to its rift (Fodor and Vetter 1984, Mizusaki *et al.* 1992), post-rift (Dani *et al.* 2017),

and drift (Rangel 2006) sedimentary megasequences (Fig. 2). The drift sedimentary sequence in Campos Basin records marine sedimentation due to the connection between the South Atlantic, North Atlantic, and Indian oceans at the Upper Cretaceous and open sea conditions (Guardado *et al.* 1989, Chang *et al.* 1992). The marine sedimentation was controlled by halocinesis and a progressive increase in bathymetry (Winter *et al.* 2007). The Macaé Group (Lower Albian; Fig. 2) represents the deposition under hot and dry climate conditions in a shallow hypersaline marine environment (up to 200 m deep; Guardado *et al.* 1989). The siliciclastic-carbonate sedimentation resulted from the progressive drowning of the carbonate platform (Winter *et al.* 2007). A transgressive marine sedimentary environment under a hot, wet climate is recorded at the basal sequence of the Campos Group (Fig. 2). Water depths varied from upper (200–1,000 m) to lower (1,000–4,000 m) bathial levels and reached 2,000 m in the central areas of Campos Basin (Guardado *et al.* 1989, Winter *et al.* 2007). The hemipelagic, near-shore, fine-grained sedimentation of marls and shales of the Ubatuba Formation is interbedded with the sandstones of the Carapebus Formation. The latter represents turbiditic debris flows along large canyons whose main source was the Serra do Mar mountain range (Fig. 1) on the continent (Guardado *et al.* 1989, Winter *et al.* 2007, Castro and Picolini 2014). Turbidites are the main hydrocarbon reservoir rocks in the Campos Basin, particularly in its central parts, such as in the Roncador and Marlin petroleum fields.

Alkaline basalts, diabases, and gabbros ranging from *ca.* 85 to 80 Ma and minor hyaloclastites and bentonites are the representative lithotypes of the Santonian-Campanian magmatic



Source: modified from Almeida *et al.* (2021).

**Figure 1.** Location of well 1-BRSA-37-RJS in Campos Basin in the continental margin of SE Brazil. Roncador and Marlim Sul oil fields and Cabo Frio Structural High that separate Campos from Santos (to the south) basins are indicated.

event in Campos Basin (Fig. 2; Mizusaki *et al.* 1992, Winter *et al.* 2007). The bentonites were formed from the alteration of volcanic ash deposits related to subaerial Plinian volcanism of

trachytic affinity that occurred in the continental area (Caddah *et al.* 1994). These bentonites are a stratigraphic marker bed in the basin, similarly to the radioactive pelitic rocks formed by

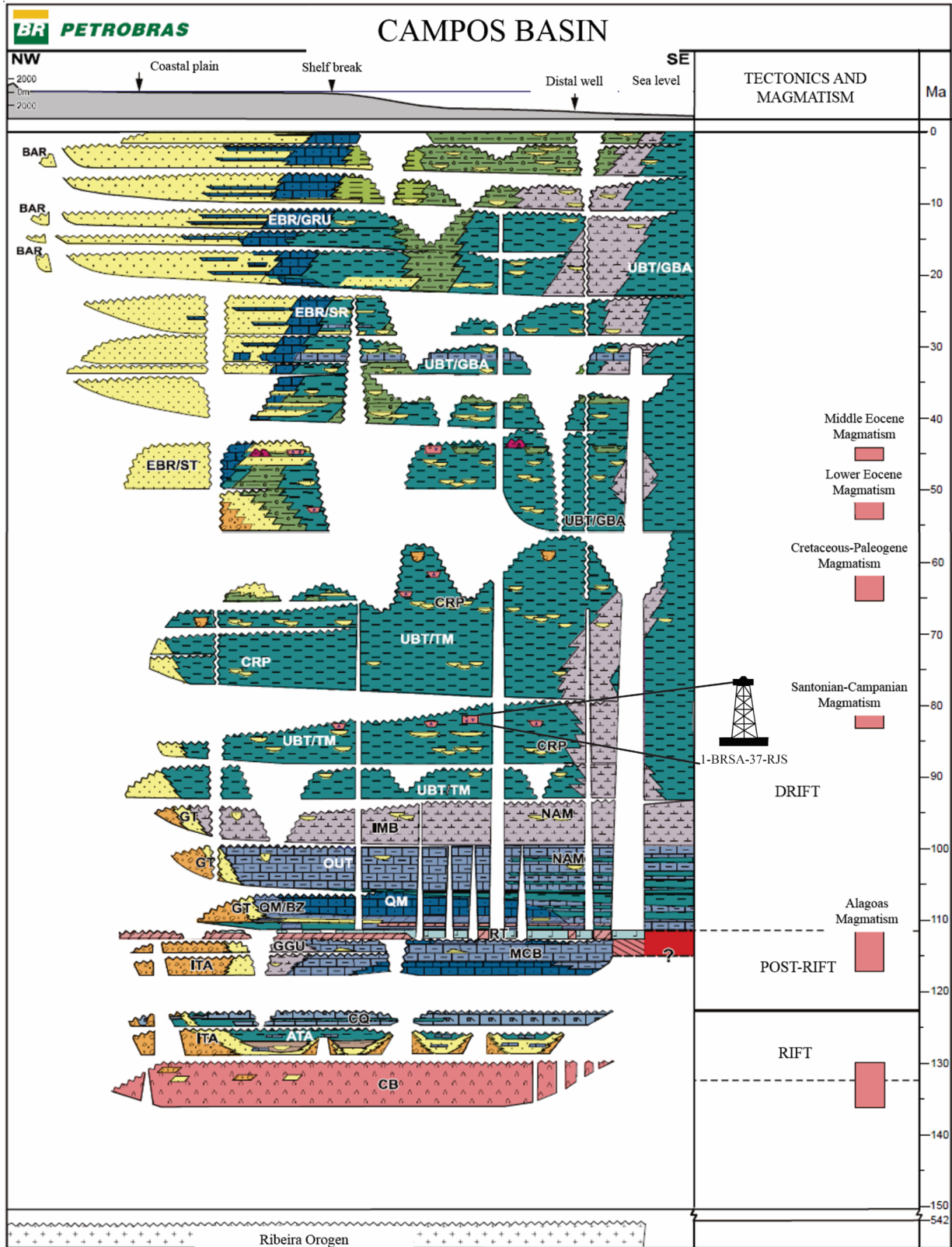


**Figure 2.** Chronostratigraphic chart of the Campos Basin (Winter *et al.* 2007). The oil well icon indicates the approximate position of the volcanoclastic interval in the Santonian-Campanian sequence. Formations and members are as follows: CB: Cabiúnas Formation, ITA: Itabapoana Formation, ATA: Atafona Formation, CQ: Coqueiros Formation, GGU: Gargau Formation, MCB: Macabu Formation, RT: Retiro Formation, GT: Goitacás Formation, QM: Quissamã Formation, BZ: Búzios Member, OUT: Outeiro Formation, NAM: Namorado Formation, IMB: Imbetiba Formation, UBT: Ubatuba Formation, TM: Tamoios Member, CRP: Carapebus Formation, EBR: Emboré Formation, ST: São Tomé Member, GBA: Geribá Member, SR: Siri Member, and GRU: Grussaí. The question mark refers to the location of the continent-ocean crust boundary.

reworked volcanoclasts and basal detrital sediments coming from the dismantling of the proximal deposits of volcanoes adjacent to the basin (Alves 2006). The turbiditic sedimentation in Campos Basin during the Santonian-Maastrichtian may have been controlled by volcanism and related seismicity in the continental margin, triggering turbidity currents (Caddah *et al.* 1998). The contemporaneity between the Santonian-Campanian volcanic processes on the continent and turbidite sedimentation is indicated by the presence of volcanic fragments in deepwater turbidite reservoirs in Campos Basin (Caddah *et al.* 1998, Fetter *et al.* 2009).

Magmatic structures were discriminated in the Campos and Santos basins, particularly along the Cabo Frio Structural High, based on seismic facies (Moreira *et al.* 2006, Oreiro 2006; Table 1). Lava flows of amygdaloidal basalts in depositional depressions with volcanoclastic breccia at the base, as well as pyroclastic deposits, occur in the Santonian-Campanian depositional sequence in the Cabo Frio Structural High area (Moreira *et al.* 2006). Cones are preferentially aligned along an E–W trend and have average dimensions of 25 km<sup>2</sup> in area and 700 m in height, being fed by subvertical to vertical dykes, associated ring dykes, and sills, according to the interpretation of seismic data obtained in southern Campos (Mohriak 2003, Moreira *et al.* 2006, Oreiro *et al.* 2008). Paleogeographic studies suggest that the volcanism was subaerial in the proximal portions and subaqueous in the distal portions of the basin. Various different intrusive and extrusive structures were discriminated by the interpretation of seismic data in the southern Campos and northern Santos (Rancan *et al.* 2018, Ren *et al.* 2019) and were included in the Santonian-Campanian volcanic phase of these basins (Schattner and Mahiques 2020). Previous works (Moreira *et al.* 2006, Oreiro 2006) have characterized the Santonian-Campanian volcanism in the area near the Cabo Frio Structural High (K90 sequence between unconformities at 88.5 Ma and 79.2 Ma) as subaerial and subaqueous, whose volcanic cones and intrusive and effusive rocks provided crystals and lithoclasts to the siliciclastic sedimentary rocks. The biostratigraphy of the sediments within sequence K90 has also given Santonian-Campanian ages (Moreira *et al.* 2007). Table 1 summarizes the main features of the Santonian-Campanian volcanism in these areas based on seismic facies, log-facies, and lithological studies.

The Eocene alkaline magmatism in Campos (Oreiro 2006, Rangel 2006, Oreiro *et al.* 2008, Mohriak and Fainstein 2012) is well recorded in the Cabo Frio Structural High area (Fig. 1). The Eocene magmatic rocks were included in the Cabo Frio Member as part of the Emborê Formation (Fig. 2), which is characterized by a thick volcano-sedimentary sequence interbedded with alkaline basaltic intrusions and lava flows (Oreiro 2006, Ren *et al.* 2019) dated at 53 Ma and 43 Ma (Mizusaki and Mohriak 1993, Winter *et al.* 2007). Epiclastic rocks, autoclastic breccias, pyroclastic tuffs, and hyaloclastites interbedded with shales, siltstones, and calcisiltites compose the volcanoclastic sequence and record periods of quiescence alternating with volcanic activity. Hyaloclastites were formed in a subaqueous environment at depths of up to 500 m (Mizusaki and Mohriak 1993, Rangel 2006, Mohriak 2020). Vertical to subvertical feeder, dykes and volcanic edifices are structures frequently observed in the seismic sections of the Eocene sequence at the Cabo Frio Structural High area (Mizusaki and Mohriak 1993, Mohriak 2003, Rangel 2006, Oreiro *et al.* 2008, Marcondes 2010), the latter being often conical but also top planar as a result of subaerial exposure from water depths of around 600 m (Oreiro 2006). In addition, “saucer-shaped” sills and basaltic flows were also recognized in the Eocene section of seismic profiles (Moreira *et al.* 2006, Oreiro *et al.* 2008), and alkaline lamprophyre and phonolite shallow intrusions with  $38.62 \pm 0.02$  Ma and  $41.06 \pm 0.02$  Ma, respectively, occur in the pre-salt section of the Cabo Frio Structural High area (Louback *et al.* 2021).

## MATERIALS AND METHODS

Well 1-BRSA-37-RJS was drilled in the south area of Campos Basin, nearby the Cabo Frio Structural High area. Well section and cutting samples, as well as gamma-ray, resistivity, neutrons, density, and sonic profiles data obtained during drilling, were made available by the National Petroleum Agency of Brazil (ANP). Cutting samples obtained at 3-m intervals were chosen for selection, with an exception made for depths 6, 9, and 12 m from the top, whose samples were not made available by ANP (Fig. 3). Paleontological studies of nanofossils in the sedimentary rocks of the studied well allow us to relate this sampled interval with the Santonian magmatic event recorded

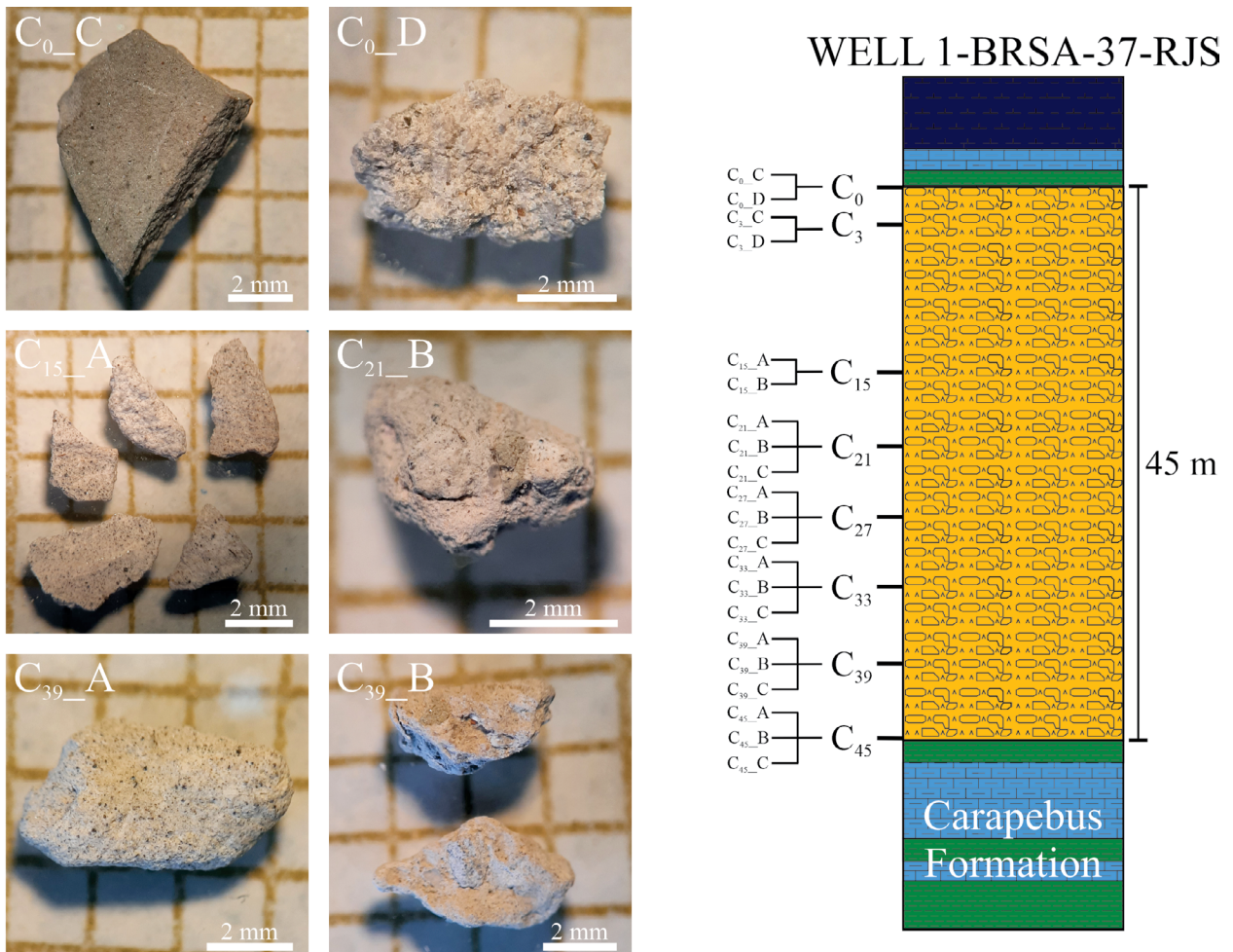
**Table 1.** Main features of the Santonian-Campanian volcanism in NE Santos (Caddah *et al.* 1994, Alves 2006, Moreira *et al.* 2006, Oreiro 2006).

Structure	Features
VC	Individual cones are 500–800 m high (average 700 m) and cover 25 km <sup>2</sup> . Cones with no internal seismic reflections and cones with strong contrasts in seismic amplitude (implying the presence of rocks with different densities). Seismic 3D visualization shows a relationship between volcanic cones formed by different lava pulses and basaltic flows, the latter filling topographic lows in the basin. Volcanic conduits extend down to the basement of the basin. Volcanic ashes interbedded with Santonian shales (Marco 3-Dedos) are ash falls from subaerial volcanism in the adjoining continental area.
F	Sampled in wells drilled in Santos ( <i>e.g.</i> , well SAN-1). Amigdaloidal basalts (high Ti contents) interbedded with siliciclastic rocks. Strong contrast of negative acoustic impedance. Log-facies: low gamma-ray values, high resistivity, and high density (4,500 m/s). Sampled greenish-gray, coarse-grained, volcanoclastic breccias were related with low gamma-ray values, low resistivity, and low density (3,400 m/s) and associated with pyroclastic flows.
I	Dikes display inclined strong positive and negative acoustic impedance. Extensions can reach 1,500 m. Sills are saucer-shaped and samples were dated at 48.9 Ma (younger than the Santonian-Campanian magmatism). Log-facies are indistinguishable from flows (F).

VC: volcanic cones; F: flows; I: intrusive rocks.

in Campos Basin (Winter *et al.* 2007). Samples were sieved, and the fraction above 14# was set aside. This fraction was washed first under tap water and then dried in the air. After drying, the cutting samples were divided into aliquots according to textural and color criteria using a binocular stereoscope, reaction under 6M HCl, and magnetic attraction. A total of 15 thin sections were done with 21 aliquots of selected cutting samples. The thin sections were then described under the transmitted light microscope (ZEISS) of the Department of Petrology and Geotectonics at UFRRJ and photomicrographs were taken. The petrographic descriptions allowed the selection of two aliquots of cutting samples from the studied interval to be powdered for whole-rock geochemical analysis. The criteria for this selection were the low degree of alteration and the representativeness of the samples. Before comminution, the cutting samples were washed in an ultrasonic cleaning device, the Yaxun YX-2050, to eliminate any remaining drilling fluid or other contaminant materials. Washing was done at room temperature for a variable time depending on the control through the inspection under the stereoscope. Finally, samples

were washed a final time under distilled water and put to dry in the air. Whole-rock geochemical analyses were obtained at Activation Laboratories Ltd. (Actlabs, Canada) on fused samples. Major element concentrations ( $\text{SiO}_2$ ,  $\text{TiO}_2$ ,  $\text{Al}_2\text{O}_3$ ,  $\text{Fe}_2\text{O}_3$ ,  $\text{MnO}$ ,  $\text{MgO}$ ,  $\text{CaO}$ ,  $\text{Na}_2\text{O}$ ,  $\text{K}_2\text{O}$ , and  $\text{P}_2\text{O}_5$ ; in wt.%;  $\text{Fe}_2\text{O}_3$  being total iron as ferric iron) were performed by inductively coupled plasma optical emission spectrometry (ICP-OES) in a Thermo Jarrell Ash ENVIRO II apparatus. Calibration was performed using 14 prepared USGS and CANMET-certified reference materials. One of the 14 standards was used during the analysis for every group of 10 samples. The selected trace elements (Ba, Rb, Sr, Zr, Y, Nb, Ni, Cr, V, Co, U, Th, Hf, Ta, and Pb), including the whole set of rare earth elements (La, Ce, Pr, Nd, Sm, Eu, Gd, Tb, Dy, Ho, Er, Tm, Yb, and Lu), were determined (in ppm) by inductively coupled plasma mass spectrometry (ICP-MS) in a Perkin Elmer Sciex ELAN 9000. Three blanks and five controls (three before the sample group and two after) were analyzed per group of samples. Duplicates are fused and analyzed every 15 samples. The loss on ignition was measured by percentual weight loss after heating at 1,100°C



LITHOLOGY

- Volcanoclastic rocks      Calcilutite      CUTTING SAMPLES
- Shale      Marl

**Figure 3.** Volcaniclastic section of well 1-BRSA-37-RJS in Campos Basin. Sedimentary rocks below and above the volcaniclastic section are also shown. Lithologies taken from the drilling section of well 1-BRSA-37-RJS provided by ANP.

for two hours. The detection limits for the major elements were 0.01 wt.% except for MnO (0.001 wt.%). The detection limits for the trace elements were as follows: Ni (20 ppm), Cr (20 ppm), Sc (1 ppm), Co (1 ppm), V (5 ppm), Ba (2 ppm), Rb (1 ppm), Sr (2 ppm), Y (0.5 ppm), Zr (1 ppm), Nb (0.2 ppm), U (0.01 ppm), and Th (0.05 ppm). The detection limits for the whole set of rare earth elements (REE) were below chondrite values. Accuracy and precision for major elements were below 3% and below 1.5%, respectively. Accuracy values for Ni, Cr, Sc, Co, and V were between 2.9 and 8.8%, whereas Y and Nb were 8.4 and 5.1%, respectively. Values for Rb and Sr were 4.8 and 1.4%, respectively, whereas Zr and Ba were 16.1 and 11.6%, respectively. Accuracy values for REE were between 1.8 and 9%, except for La (10.6%). The values for U and Th were 3.8 and 4.2%, respectively. Precision values for Cr, Sc, Co, and V were between 0.5 and 9.1%, except for Ni (11.1%), whereas Y, Zr, and Nb were below 1.9%. Values for Rb, Ba, and Sr were between 0.5 and 8.8%. Precision values for the REE were between 2.1 and 8.7%, except for Eu (12.1%). Values for U and Th were 5.4 and 3%, respectively.

## RESULTS

### Well data and log-facies discrimination

The volcanoclastic succession observed in well 1-BRSA-37-RJS is 45-m thick (Fig. 3). Coherent variations of geophysical borehole data (gamma-ray, resistivity, neutron, density, and sonic) were qualitatively evaluated so that they could be further related to petrographic data obtained from samples of the representative lithologies in the studied interval. The sets of variations in borehole data comprise the hereafter-called log-facies.

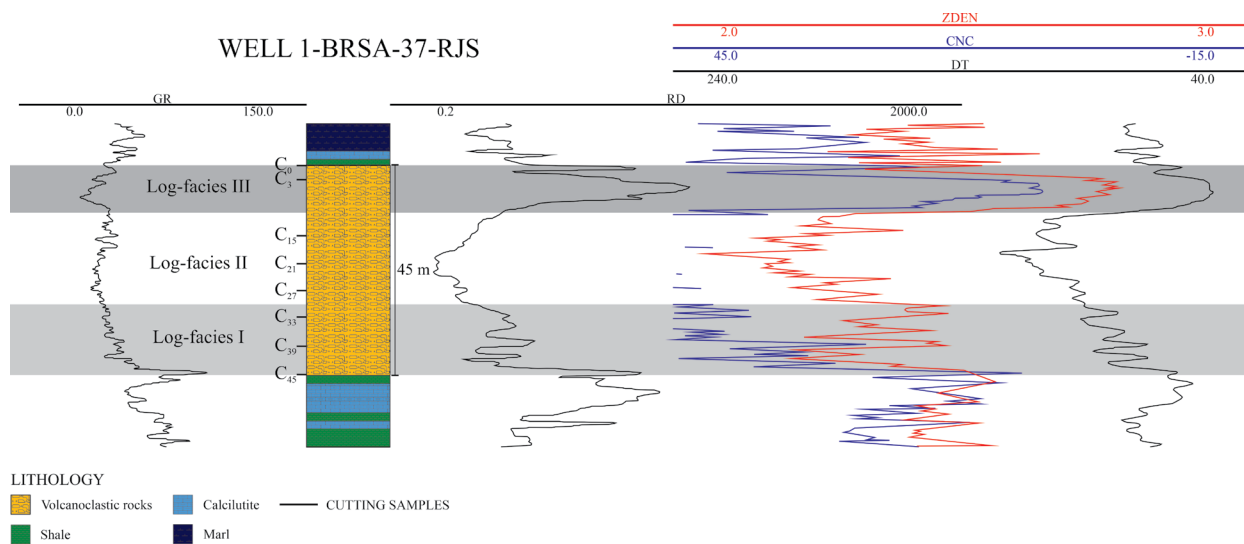
The rocks were described as tuff in the well log. Shale and calcilitite of the Carapebus Formation occur at the base and top of the Santonian-Campanian interval (Fig. 3). Four distinct lithologies were identified by selecting and describing cutting samples from the magmatic interval. These lithologies are non-magnetic and react differently in the presence of HCl (6 mol/L). The mudstone is composed of mafic minerals

and micas within a greenish-grey clay matrix (sample C<sub>0</sub>\_C, Fig. 3). The sandstone is composed of quartz and mafic minerals cemented by carbonate (sample C<sub>0</sub>\_D, Fig. 3). Two types of volcanoclastic rocks occur in this section. Black lithoclasts occur in a white carbonate matrix in a well-sorted volcanoclastic rock (samples C<sub>15</sub>\_A and C<sub>39</sub>\_A, Fig. 3). Another volcanoclastic rock comprises lithic fragments of the previously described volcanoclastic rock and lamite cemented by carbonate (samples C<sub>21</sub>\_B and C<sub>39</sub>\_B, Fig. 3). Paleontological studies of nanofossils in the sedimentary rocks allow for the correlation of this magmatic section with the Santonian magmatic event recorded in Campos Basin (Winter *et al.* 2007).

Three log-facies were discriminated in the volcanoclastic interval (Fig. 4). Log-facies I is at the base (15 m), log-facies II is at the middle portion (20 m), and log-facies III is at the top of the volcanoclastic section (10 m). The gamma-ray values of the three log-facies are low, with symmetrical and box-shaped patterns (Fig. 4). Log-facies I is characterized by a low amplitude and low wavelength oscillation in the resistivity, neutron, density, and sonic data combined with the highest gamma-ray values. Log-facies II displays slightly higher amplitude oscillations with higher neutron and sonic values combined with lower resistivity and density values when compared with log-facies I. Log-facies III is opposite to log-facies I and II, displaying the highest amplitude and wavelength oscillations that combine high values in the resistivity and density profiles with low values in the neutron and sonic data (Fig. 4).

### Petrography

There is a sizeable lithological variety in the volcanoclastic interval analyzed in well 1-BRSA-37-RJS. The rocks were classified by following, as much as possible, the recommendations proposed by the International Union of Geological Sciences (IUGS) (Le Maitre *et al.* 2002). However, slight modifications to the IUGS classification of the mixed deposits were necessary. The classification used in this work (Table 2) is non-genetic and based only on grain size and the presence of any material of volcanic origin (rock or individual crystal fragment), regardless of the fragmentation and deposition mechanism. The term



GR: gamma-ray log; RD: resistivity log; CNC: neutron log; DT: sonic log; ZDEN: density log.

**Figure 4.** Borehole logs and discriminated log-facies in well 1-BRSA-37-RJS.

tuffaceous is added as a qualifier to the grain size nomenclature (*i.e.*, breccia, conglomerate, sandstone, siltstone, and mudstone) for rocks containing between 50 and 25% by volume of material of volcanic origin. Similarly, the term epiclastic is added to the grain size nomenclature for rocks with less than 25% by volume of material of volcanic origin. This classification does not take into account the volume of matrix or cement.

Four lithotypes were classified from 15 thin sections of 21 selected aliquots of cutting samples from the studied well (Fig. 3). Cutting samples of predominant volcanoclastic rocks (deeper than C15; Fig. 3) were obtained at the base and middle portions of the section, corresponding to log-facies I and II (Fig. 4). On the contrary, sedimentary rocks (shallower than C15; Fig. 3) prevail at the top of the interval and correspond to log-facies III (Fig. 4).

The volcanoclastic rocks are a tuffaceous siltstone and an epiclastic siltstone (Table 2). The tuffaceous siltstone is composed of subangular grains of quartz, carbonate, opaque minerals, and olivine, as well as subangular to subrounded volcanic rock fragments dispersed in a microcrystalline carbonate (Fig. 5A). The volcanic rock fragments are hypohyaline, inequigranular, very fine (< 0.1 mm), with euhedral to

subhedral prismatic, columnar and hexagonal minerals, and a glassy aphanitic groundmass (Fig. 5B). The tuffaceous siltstone is well sorted, and the partial dissolution of the matrix generated a secondary porosity in this rock.

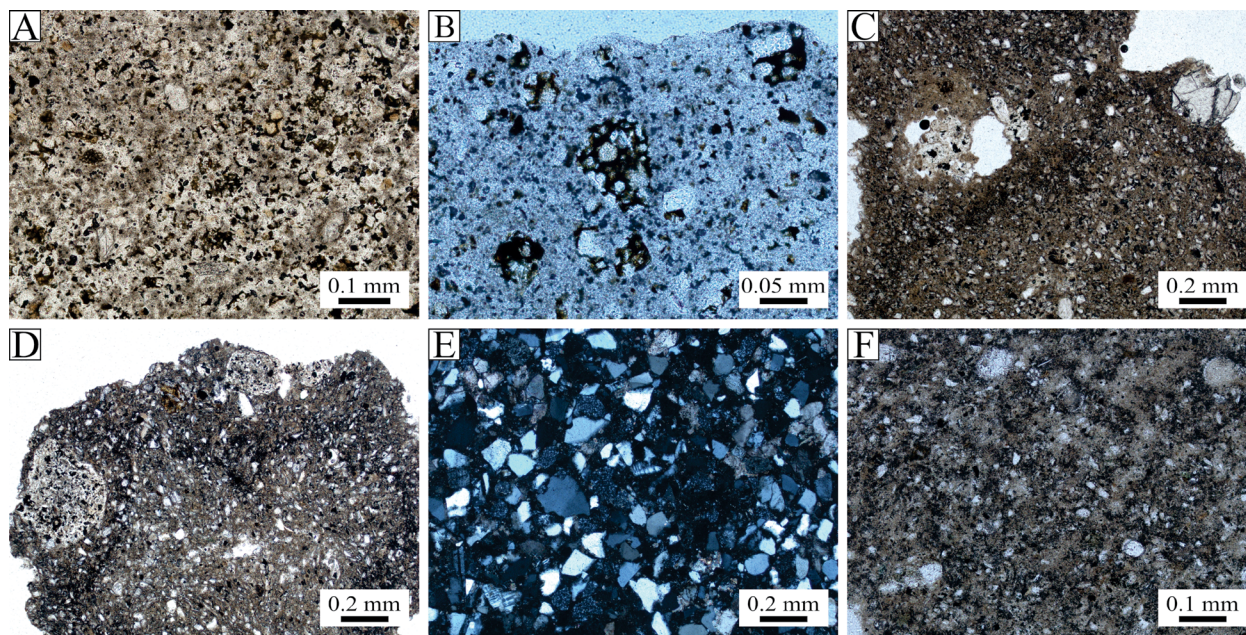
The epiclastic siltstone is well sorted and composed of subangular grains of carbonate, quartz, feldspar, mica, opaque minerals, rutile, zircon, and olivine (Fig. 5C); bioclasts; and rounded lithic fragments of tuffaceous siltstone and fossiliferous mudstone (Fig. 5D), all cemented by carbonate. At the top of the section, sedimentary rocks predominate, comprising arkose and fossiliferous mudstone. The arkose is well sorted and composed of subangular grains of quartz, feldspar (microcline and plagioclase), mica, opaque minerals, rutile, and zircon, as well as subangular to subrounded sedimentary rock fragments cemented by silica- and carbonate-rich material (Fig. 5E).

The presence of microclines indicates a provenance related to the Proterozoic basement (Fig. 1), mostly composed of gneisses of granitic composition. The fossiliferous mudstone (Fig. 5F) consists of a clay mineral-rich matrix and subangular to subrounded grains of quartz, carbonate, feldspar, opaque minerals, mica, rutile, and zircon. Allochemical grains that include bioclasts and pellets occur in abundance in this rock.

**Table 2.** Terminology for volcanoclastic rocks used in this work.

		Mixed Deposits	
wt.% material of volcanic origin (mm)		50–25	< 25
	Gravel > 2	Tuffaceous conglomerate, tuffaceous breccia	Epiclastic conglomerate, epiclastic breccia
Grain size	Sand 2–0.0625	Tuffaceous sandstone	Epiclastic sandstone
	Silt 0.0625–0.0039	Tuffaceous siltstone	Epiclastic siltstone
	Clay < 0.0039	Tuffaceous mudstone	Epiclastic mudstone

Source: modified after Le Maitre *et al.* (2002).



PPL: plane-polarized light; CPL: cross-polarized light.

**Figure 5.** Photomicrographs of representative samples in well I-BRSA-37-RJS in Campos Basin. (A) Abundant volcanic rock fragments and microcrystalline carbonate matrix in the tuffaceous siltstone (Sample C<sub>45</sub>\_A, PPL). (B) Volcanic rock fragments in detail in tuffaceous siltstone (Sample C<sub>39</sub>\_A, PPL). (C) Olivine grain and tuffaceous siltstone fragment in the epiclastic siltstone (Sample C<sub>21</sub>\_B, PPL). (D) Well-sorted epiclastic siltstone with fragments of tuffaceous siltstone (Sample C<sub>27</sub>\_B, PPL). (E) Well-sorted, sub-angular, sandstone arkose (Sample C, C<sub>0</sub>\_D, CPL). (F) Abundant allochemical grains in the fossiliferous claystone (Sample C<sub>33</sub>\_C, PPL).

## Lithogeochemistry

Two aliquots of cutting samples from well 1-BRSA-37-RJS were analyzed for whole-rock geochemical analysis (Table 3). The criteria for this selection were the low degree of alteration and the representativeness. The analyzed samples have very high loss on ignition (LOI) values, as expected for volcanoclastic and epiclastic rocks. The high CaO values and, to a lesser extent, the low LOI values are consistent with the high

**Table 3.** Lithogeochemical data of tuffaceous siltstone (sample C-1) and epiclastic siltstone (sample C-2) in well 1-BRSA-37-RJS in Campos Basin. Fe<sub>2</sub>O<sub>3</sub><sup>(T)</sup> is total iron, also known as ferric iron. LOI is loss on ignition. Oxides in wt.%. Elements in ppm. b.d.l. is below the detection limit.

	C-1	C-2		C-1	C-2
SiO <sub>2</sub>	18.41	21.47	Zr	39	82
TiO <sub>2</sub>	0.21	0.30	Nb	3	11
Al <sub>2</sub> O <sub>3</sub>	4.53	4.58	La	8.1	18.0
Fe <sub>2</sub> O <sub>3</sub> <sup>(T)</sup>	4.68	2.59	Ce	13.9	33.4
MgO	2.10	1.98	Pr	1.78	3.54
MnO	0.06	0.05	Nd	6.88	12.30
CaO	34.27	23.17	Sm	1.34	2.42
Na <sub>2</sub> O	0.40	0.45	Eu	0.42	0.58
K <sub>2</sub> O	1.07	1.16	Gd	1.30	1.74
P <sub>2</sub> O <sub>5</sub>	0.17	0.13	Tb	0.20	0.28
LOI	32.13	26.02	Dy	1.17	1.48
Total	98.04	81.89	Ho	0.25	0.30
Ni	40	b.d.l.	Er	0.65	0.83
Cr	130	40	Tm	0.096	0.113
Sc	5	5	Yb	0.65	0.75
Co	5	2	Lu	0.105	0.117
V	54	35	Hf	0.9	1.9
Rb	8	37	Pb	58	18
Ba	3,133	107,200	Th	1.11	3.65
Sr	671	2,669	U	3.30	1.32
Y	8	8			

amount of carbonate in the matrix of those rocks. The very high Ba contents are may be due to contamination by drilling fluids, despite the careful cleaning procedures adopted during sample preparation.

The tuffaceous siltstone (sample C-1) and the epiclastic siltstone (sample C-2) of well 1-BRSA-37-RJS are classified as alkaline basalt and basalt on the Zr/TiO<sub>2</sub> versus Nb/Y and Zr/Ti vs. Nb/Y diagrams, respectively (Fig. 6).

The trace element patterns of the tuffaceous siltstone and epiclastic siltstone in the studied well display peaks at K, Sr, and P in chondrite-normalized multi-element diagrams (Fig. 7A). The epiclastic siltstone is more enriched in the whole set of mobile and immobile trace elements than the tuffaceous siltstone, including the rare earth elements (REE; Fig. 7B). Both rocks are richer in the light REE than the heavy REE (e.g., [(La/Yb)<sub>N</sub>] > 8), although the tuffaceous siltstone and the epiclastic siltstone can be distinguished by their different [(La/Eu)<sub>N</sub>] ratios (4.6 and 7.4, respectively; Fig. 7B). The enriched trace element patterns of the tuffaceous siltstone and epiclastic siltstone indicate a provenience from continental crust sources, despite the fact that mixing processes must be considered in their petrogenesis.

## DISCUSSION

### Correlations between log-facies and petrography

Three log-facies (I, II, and III) were discriminated in the magmatic-related interval of well 1-BRSA-37-RJS (Fig. 4). Volcaniclastic (tuffaceous siltstone and epiclastic siltstone) and sedimentary rocks (arkose and fossiliferous mudstone) comprise the volcaniclastic section. Log-facies I and II are consistent with the physical and chemical properties of the volcaniclastic rocks that occur in the studied well (Rider 1996, Schön 2015). For instance, the low and fairly constant values of the gamma-ray data are in agreement with the presence of carbonate matrix and cement in the tuffaceous siltstone (Figs. 5A and 5B) and epiclastic siltstone (Figs. 5C

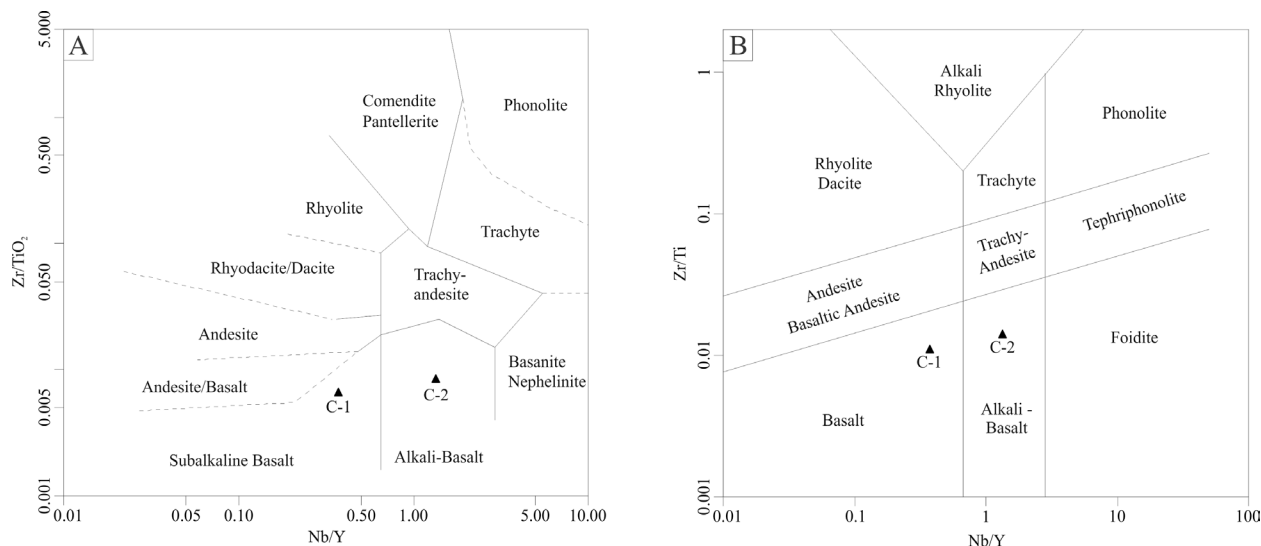


**Figure 6.** Classification diagram of well 1-BRSA-37-RJS. (A) Zr/TiO<sub>2</sub> vs. Nb/Y (Winchester and Floyd 1977). (B) Zr/Ti vs. Nb/Y (after Winchester and Floyd 1976; modified by Pearce 1996).

and 5D), respectively. The low values of the gamma-ray profile can also be associated with the presence of subangular grains of olivine and subangular to subrounded fragments of volcanic rock, suggesting a mafic composition for the igneous source. These mineral grains and fragments may be the result of erosion and transport of erupted basalts from subaerial volcanic edifices discriminated in the southern Campos Basin based on geophysical data (Mohriak 2003, Moreira *et al.* 2006, Winter *et al.* 2007, Oreiro *et al.* 2008), given the well-sorted texture of volcanoclastic rocks. Oscillation at different scales in the resistivity, neutron, density, and sonic profiles of log-facies I and II indicates interlayering of materials with different properties (*e.g.*, Zou *et al.* 2013). The low resistivity and density values, associated with the high values in the neutron and sonic profiles, indicate that the rock is porous and not very dense. These properties were observed in the tuffaceous siltstone throughout macroscopic analysis (Fig. 3) and petrography (Figs. 5A and 5B). The high values of resistivity and density, combined with low values in the neutron and sonic profiles of log-facies I compared to log-facies II, indicate that the rock at the bottom of the section is massive and consists of more resistive minerals such as carbonate (Schön 2015). These properties were observed in the epiclastic siltstone (Figs. 5C and 5D). According to log-facies and petrographic interpretation, it is possible to suggest a stratigraphy represented by the interbedded tuffaceous siltstone and epiclastic siltstone, the latter prevailing at the bottom of the volcanoclastic section on the studied well (Fig. 3). In addition, the presence of fragments of tuffaceous siltstone in the epiclastic siltstone (Figs. 5C and 5D) suggests that these lithologies were deposited at different times and that the epiclastic siltstone corresponds to a subaerial

reworking of the volcanoclastic deposit itself and, to a lesser extent, also of the magmatic source region.

The main drawback regarding correlations between petrographic and well log data is seen at the top of the studied section (log-facies III), particularly with the resistivity data. For instance, low neutron and sonic data associated with high density values are not often related to siliciclastic sequences. In addition, resistivity values are just too high in the top, siliciclastic portion of the well. However, despite its successful use for correlation, resistivity data is influenced by changes in formation pressure and interstitial water salinity, which are non-stratigraphic, post-depositional elements that tend to obliterate the original depositional features (Rider 1996).

## Volcanosedimentary paleoenvironment

Subaerial and subaqueous volcanic cones were distinguished in the area and were related to shallow- and deep-sea water system tracts, respectively. The fragments of basaltic rocks and olivine in the tuffaceous siltstone identified in cutting samples of the studied interval from well 1-BRSA-37-RJS indicate the sole contribution from a subaerial volcanic source. No fragments of hydroclasts and hyaloclastites that could be related to the provenience of a subaqueous volcanic source have been described in the analyzed volcanoclastic rocks. Parts of the lithoclasts in the tuffaceous siltstone are highly vesicular, being classified as scoria basalts, implying either subaerial volcanism or shallow-water volcanism since high hydrostatic pressure prevents vesiculation in lavas. No lithoclasts of evolved lithotypes were found, nor were felsic minerals of volcanic origin, such as high-temperature alkaline feldspar or quartz. More likely, the volcanic and mineral fragments in the volcanoclastic rocks seem to be associated with subaerial scoria and spatter cones similar to the Paricutin volcano (Inbar *et al.* 1994; Fig. 8) rather than hydrovolcanic tuff rings, tuff cones, or maars. Scoria cones comprise both volcanoclastic (small explosions) rocks and restricted lava flows, the latter effused mostly from fissure zones at the base of the cone (Fig. 8; Table 1). They are small, poorly stratified structures (< 200–700 m high; bases with ~500 m in diameter) underlain by long feeder conduits, usually aligned along fault systems where they group as tens or hundreds of cones in monogenetic volcanic fields (Hasenaka and Carmichael 1985, Németh 2010, Kereszturi and Németh 2012). These features are similar to those described for the volcanic cones in northern Santos (Table 1). Subaerial volcanism must have occurred in a near-shore setting under shallow water depths. The siliciclastic rocks associated with the volcanoclastic are arkose and fossiliferous mudstone. The subangular shape of siliciclasts in the arkose, whose feldspars are mostly microcline, indicates a proximal source such as the granites and orthogneisses that crop out along the Serra do Mar mountain range in the continental area adjoining the southern Campos Basin. The petrographic features of the sedimentary and volcanoclastic rocks in the study area indicate a volcanosedimentary paleoenvironment located in a near-shore area such as the continental shelf, as opposed to the continental slope or rise where subaqueous volcanism and turbiditic processes would have taken place in the Santonian-Campanian in southern Campos Basin (Fig. 9).

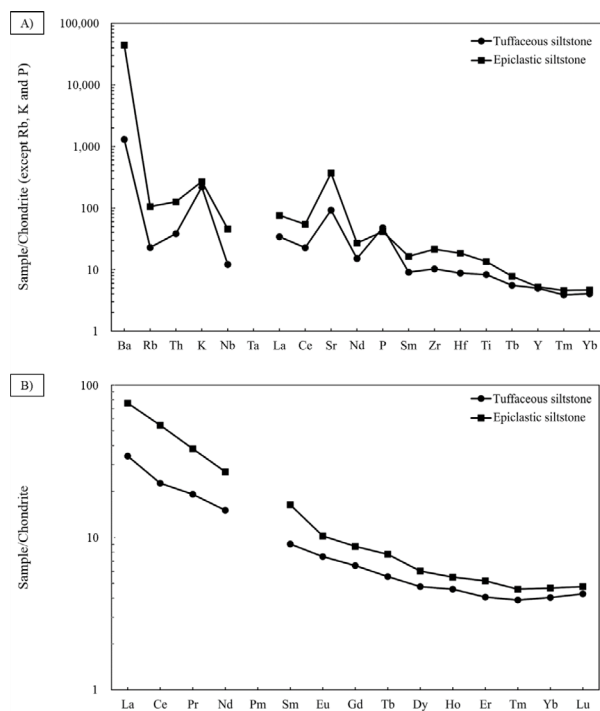


**Figure 7.** Trace element patterns of the volcanoclastic and epiclastic rocks in well 1-BRSA-37-RJS. (A) Chondrite-normalized multielement diagram. (B) Chondrite-normalized REE diagram. Normalization factors from McDonough and Sun (1995), except Rb, K, and P (primitive mantle from Sun 1980).

### Volcaniclastic rocks as probes of the mantle

In general, volcaniclastic rocks can be taken as the products of volcanic rocks by weathering, transportation, and redeposition that are mixed with sedimentary debris (e.g., Fisher 1961, McPhie *et al.* 1993, Le Maitre *et al.* 2002, White and Houghton 2006, Manville *et al.* 2009). As such, the lithochemical composition of the volcaniclastic rocks may inherit those of their contributing sources. Major element compositions are more suitable to be modified by diagenetic and post-magmatic processes. The same applies to the large ion lithophile trace elements such as Rb, Ba, and Sr. On the contrary, the highfield-strength trace elements such as Zr, Y, Ti, and Nb and most of the REE are immobile during post-magmatic processes and retain the characteristics of their sources. The REE are insoluble, transported as particulates, and occur in low concentrations in seawater and river waters. Weathering can modify REE concentrations, but they are promptly precipitated at the weathering site. Diagenesis is also unlikely to

change REE concentrations because it would require a high water/rock ratio setting. On the contrary, psammitic, quartz-rich sediments tend to dilute the REE concentrations, as do carbonate-rich rocks. In addition, the REE concentrations are erratically modified due to the concentrations of REE-rich minerals such as zircon, monazite, and allanite. The HFSE and REE smooth patterns of the tuffaceous siltstone and epiclastic siltstone, free of peaks and valleys (Fig. 7), indicate that their compositions were not dramatically changed during post-magmatic, diagenetic or alteration processes. Thus, the HFSE and REE contents of sediments and volcaniclastic rocks can provide good information on provenance. In particular, it is the clay- and silt-sized fraction of the sedimentary and volcaniclastic rocks that are likely to better represent their sources (Nesbitt 1979, Fleet 1984, Cullers *et al.* 1987, McLennan 1989, Nesbitt *et al.* 1990).

The tuffaceous siltstone is composed of fragments of olivine and volcanic rock, whereas the epiclastic siltstone bears

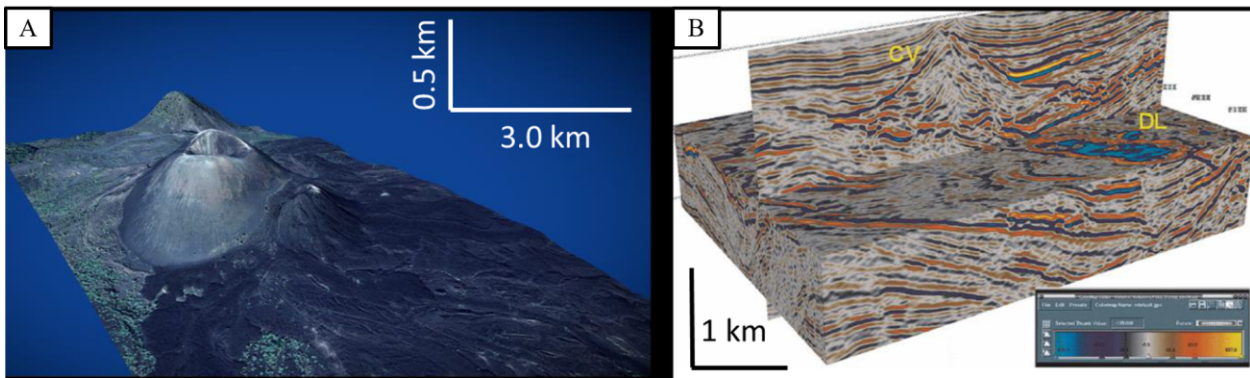


**Figure 8.** Comparisons between volcanic cones in Paricutin, Mexico, and the northern Santos Basin. (A) 3D model of the Paricutin monogenetic volcano, Mexico (<https://sketchfab.com/search?q=paricutin&type=models>). (B) 3D seismic visualization of a volcanic cone (CV) and associated lava flow (DL) in the northern Santos Basin (Moreira *et al.* 2006).

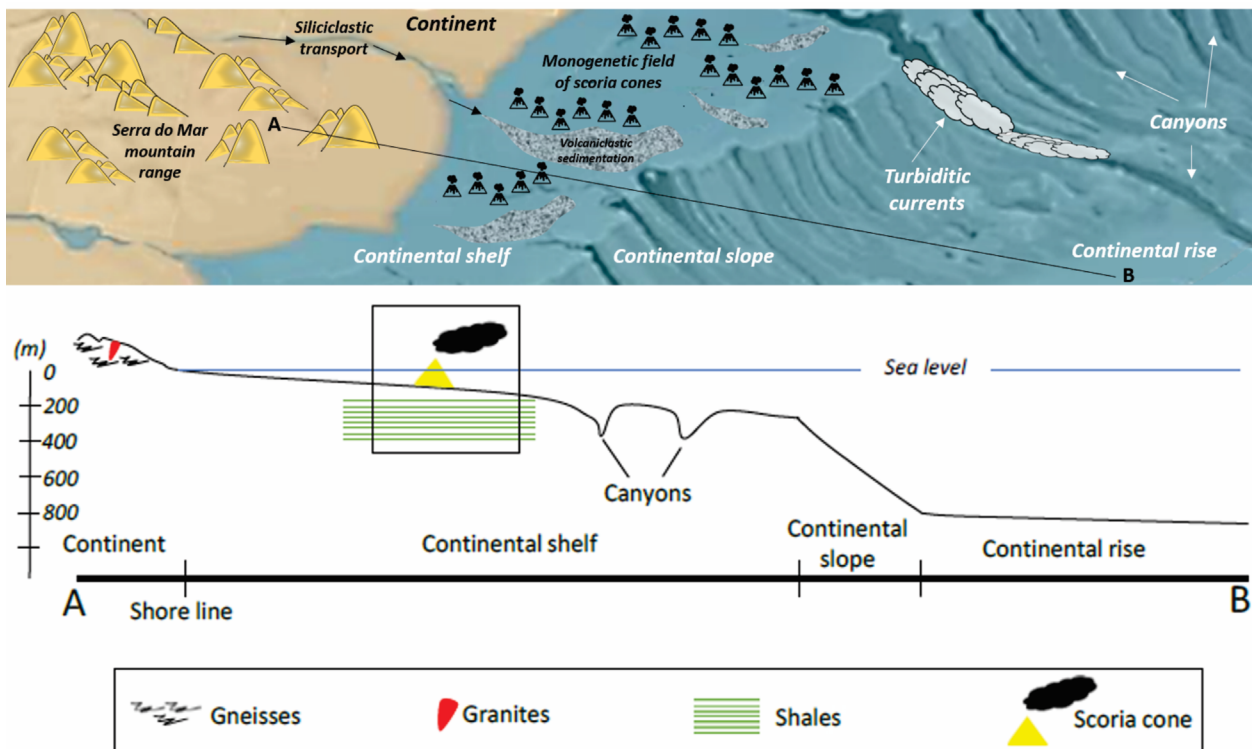


**Figure 9.** Schematic reconstruction (not in scale) of the volcanosedimentary paleoenvironment in southern Campos at the Santonian-Campanian. The background of the 3D reconstruction was modified from Doyle (2017).

fragments of mafic minerals as well as fragments of the tuffaceous siltstone itself. In general, these petrographic features are consistent with at least a contribution from a mafic, probably basaltic source. This is broadly consistent with the previously stated proposition that the studied volcanoclastic environment is related to basaltic scoria cones in monogenetic fields (Fig. 9). Possible basaltic sources for the volcanoclastic rocks are to be found in the oceanic crust (e.g., typical N-MORB or OIB; Sun and McDonough 1989) or in the continental tholeiitic basalts of the rift-related Cabiúnas Formation (Fig. 2) in Campos Basin (Fodor and Vetter 1984, Mizusaki *et al.* 1992). The other likely source to be involved in the formation of the volcanoclastic rocks is the continental crust (e.g., Taylor and McLennan 1985, Weaver and Tarney 1981).

Binary mixing calculations (Faure 1986) were done in order to derive the likely source components and their respective amounts in the volcanoclastic rocks C-1 and C-2 in the studied interval (Table 4). Modeling was done using immobile trace element ratios. Results of modeling (Fig. 10) have shown that C-1 and C-2 compositions would have to involve a contribution from the upper continental crust rather than the lower or average crust. The Campos basalts are not a suitable end-member in the mixing process. Interestingly, the mafic end-member is well represented by the compositions of mantle sources related to the oceanic crust (N-MORB and OIB). Smaller and greater amounts of the upper continental crust would have been involved in the formation of the tuffaceous siltstone and the epiclastic siltstone, respectively. It is unlikely that the amounts of end-members derived from modeling represent exact proportions in the mixing processes that led to the formation of the studied volcanoclastic rocks. Nevertheless, it seems relevant that continental and oceanic compositions have taken part in the process. Most probably, the oceanic crust was some hundred kilometers eastward in the southern Campos and could not contribute to the volcanoclasts found in the tuffaceous siltstone and epiclastic siltstone analyzed in

this work. The modeling indicates that the mantle underlying the southern Campos area in the Santonian-Campanian was probed by the less differentiated scoria basalts that contributed to the volcanoclastic rocks.

## CONCLUSION

Tuffaceous and epiclastic siltstones are volcanoclastic rocks that occur together with arkose and fossiliferous mudstone in a 45-m-thick interval of well 1-BRSA-37-RJS drilled in the southern Campos Basin, offshore SE Brazil. Petrographic and litho-geochemical data obtained for carefully selected and cleaned cutting samples were combined with previous geophysical data that discriminated the volcanic structures in the area to propose that the mafic sources of volcanoclasts found in the tuffaceous siltstone and epiclastic siltstone are related to subaerial, basaltic scoria cones. These volcanic edifices were distributed along lineaments in monogenetic fields located in the continental shelf of Campos Basin in the Santonian-Campanian. Two main sources provided lithoclasts and crystalloclasts to the volcanoclastic rocks: the upper continental crust, granites, and orthogneisses found in the Serra do Mar mountain range in the continental area adjoining Campos Basin, and possibly hundreds of scoria and spatter cones within the monogenetic field. It should be noted that paleoreconstructions based on scarce data are difficult to perform, leading to ambiguity. For instance, rounded grains are to be expected in the reworked continental sediments as opposed to the subangular ones found in the arkoses studied in the area since they were related to a shelf staging area. As such, the basaltic cones could be located at least in part on the continental basement adjoining Campos Basin. In this scenario, continental sediments and volcanoclastic material would have been transported throughout proximal canyons located near river mouths near the coastline. This would be broadly supported by the uplift of the coastal range as a result of the uprising of the asthenosphere

**Table 4.** Selected trace element contents (in ppm) of samples C-1 (tuffaceous siltstone) and C-2 (epiclastic siltstone) in well 1-BRSA-37-RJS as well as in the upper continental crust (UC), the average continental crust (AC), the lower continental crust (LC), N-MORB (normal mid-ocean ridge basalt), OIB (oceanic island basalt), and Campos basalts (Fm. Cabiúnas, Winter *et al.* 2007). UC and AC compositions from Taylor and McLennan (1985). LC composition from Weaver and Tarney (1981). N-MORB and OIB from Sun and McDonough (1989). Campos is the average composition (30 samples) from Fodor and Vetter (1984) and Mizusaki *et al.* (1992).

	Zr	Y	La	Nb	Zr/Y	La/Nb
<b>C-1</b>	39	8	8.1	3	4.9	2.7
<b>C-2</b>	82	8	18.0	11	10.3	1.6
<b>UC</b>	240	22	5	5	10.9	4.4
<b>LC</b>	202	7	5	5	28.9	4.4
<b>AC</b>	210	14	13	13	15.0	2.2
<b>N-MORB</b>	74	28	2.3	2.3	2.6	1.1
<b>OIB</b>	280	29	48	48	9.7	0.8
<b>Campos</b>	30	149	24	24	4.9	2.3

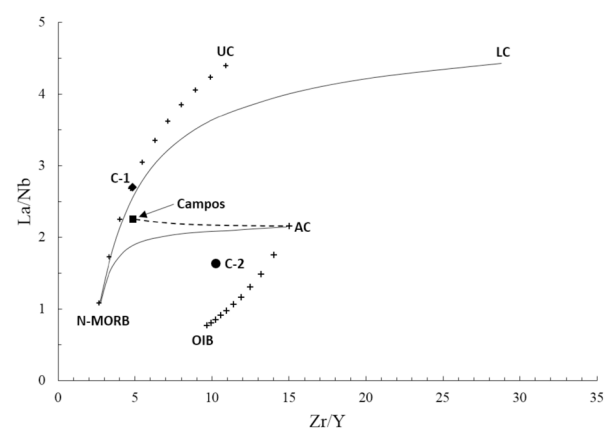


**Figure 10.** Binary mixing curves between mafic basic sources (N-MORB and Campos basalts) and continental crust compositions. Mixing curves with N-MORB, OIB, and the upper continental crust (UC) end-members at 10% intervals (crosses). Straight lines represent other mixing curves with N-MORB and OIB end-members. Dashed lines represent curves between Campos basalts and continental crust compositions. C-1 and C-2 compositions are indicated. End-members compositions and abbreviations are presented in Table 4.

as proposed in this article. Regarding mantle probing, it is suggested that the less differentiated basaltic clasts of the spatter cones may have probed the mantle underlying the area, attesting to the presence of the same sources that were giving rise to the MORB-like oceanic crust some hundreds of kilometers eastward in the southern Campos Basin. As such, this area of the basin may have been located above the melting, uprising upper mantle that could have also imparted regional discordances at the Santonian in the Campos and Santos basins, as suggested by other authors (Moreira *et al.* 2007). Petroleum

systems in southern Campos may also have been affected by the thermal influence of the uprising asthenosphere in the area.

## ACKNOWLEDGMENTS

The authors acknowledge the financial support through the R&D project, EQUIMAG (ANP 21110-2), and the Brazilian agency of petroleum (ANP) for the authorization needed to obtain the well profiles and samples. The authors also thank the reviewers for their relevant contributions to the article.

## ARTICLE INFORMATION

Manuscript ID: 20220089. Received on: 16 NOV 2022. Approved on: 28 MAR 2023.

How to cite this article: Frank Y.V.M., Valente S.C. (2023). Volcaniclastic rocks and reconstruction of a volcanosedimentary paleoenvironment in Campos Basin, SE Brazil. *Brazilian Journal of Geology*, 53(2):e20220089. <https://doi.org/10.1590/2317-4889202320220089>

Y.V.M.F.: Conceptualization, Formal analysis, Investigation, Methodology, Software, Validation, Visualization, and Writing—original draft. S.C.V.: Conceptualization, Data curation, Formal analysis, Funding acquisition, Investigation, Methodology, Project administration, Resources, Supervision, Validation, Visualization, and Writing—review & editing.

Competing interests: the authors declare no competing interests.

## REFERENCES

- Almeida J., Heilbron M., Guedes E., Neubauer F., Manfred B., Klausen M.B., Valeriano C.M., Bruno H., Giro J.P., McMaster M., Tetzner W. 2021. Pre-to-syn-rift tholeiitic magmatism in a transtensive hyperextended continental margin: Onshore and offshore magmatism of the Campos Basin, SE Brazil. *Journal of South American Earth Sciences*, 108, 103218. <https://doi.org/10.1016/j.jsames.2021.103218>
- Alvarenga R.S., Kuchle J., Iacopini D., Goldberg K., Scherer C.M.S., Pantopoulos G., Ene P.L. 2021. Tectonic and stratigraphic evolution based on seismic sequence stratigraphy: central rift section of the Campos Basin, offshore Brazil. *Geosciences*, 11(8), 338. <https://doi.org/10.3390/geosciences11080338>
- Alves D.B. 2006. Sedimentação vulcanoclástica do Cretáceo Superior da Bacia de Campos, Sudeste do Brasil. *Boletim de Geociências da Petrobras*, 14(1):149-154.
- ANP – Agência Nacional do Petróleo. 2022. *Boletim da produção de petróleo e gás natural*. ANP. Available at: <https://www.gov.br/anp/pt-br/centrais-de-conteudo/publicacoes/boletins-anp/boletins/arquivos-bmppgn/2022/boletim-junho.pdf>. Accessed on: 5 Sept. 2022.
- Armelenti G., Goldberg K., Alvarenga R., Kuchle J., Amarante F.B., Scherer C.M.S., Bastos A.C., Conceição J.C., Alves J.L.D., Deros L.F. 2021. Depositional and diagenetic impacts on the porosity of post-salt carbonate reservoirs of southern Campos Basin, southeastern Brazilian margin. *Journal of South American Earth Sciences*, 112(Part 1), 103566. <https://doi.org/10.1016/j.jsames.2021.103566>
- Caddah L.F.G., Alves D.B., Hanashiro M., Mizusaki A.M.P. 1994. Caracterização e origem do Marco “3-Dedos” (Santoniano) da Bacia de Campos. *Boletim de Geociências da Petrobras*, 8:315-334.
- Caddah L.F.G., Alves D.B., Mizusaki A.M.P. 1998. Turbidites associate with bentonites in the Upper Cretaceous of the Campos Basin, offshore Brazil. *Sedimentary Geology*, 115(1-4):175-184. [https://doi.org/10.1016/S0037-0738\(97\)00092-4](https://doi.org/10.1016/S0037-0738(97)00092-4)
- Cas R.A.F., Wright J.V. 1987. *Volcanic Successions Modern and Ancient: A geological approach to processes, products and successions*. London: Chapman and Hall, 531 p.
- Castro R.D., Picolini J.P. 2014. Principais aspectos da geologia regional da Bacia de Campos. In: Kowsmann R.O. (ed.). *Geologia e Geomorfologia*. Rio de Janeiro: Elsevier, v. 1, p. 1-12.
- Caxito F.A., Hartmann L.A., Heilbron M., Pedrosa-Soares A.C., Bruno H. Basei M.A.S., Chemale F. 2022. Multi-proxy evidence for subduction of the Neoproterozoic Adamastor Ocean and Wilson cycle tectonics in the South Atlantic Brasiliano Orogenic System of Western Gondwana. *Precambrian Research*, 376, 106678. <https://doi.org/10.1016/j.precamres.2022.106678>
- Chang H.K., Kowsmann R.O., Figueiredo A.M.F., Bender A.A. 1992. Tectonics and stratigraphy of the East Brazil Rift system: an overview. *Tectonophysics*, 213(1-2):97-138. [https://doi.org/10.1016/0040-1951\(92\)90253-3](https://doi.org/10.1016/0040-1951(92)90253-3)
- Correia U.M., Honório B.C., Kuroda M.C., Melani L.H., Vidal A.C. 2019. Geometric characterization of igneous intrusions: 3-D seismic insights from the Campos Basin, SE Brazil. *Marine and Petroleum Geology*, 102:725-739. <https://doi.org/10.1016/j.marpetgeo.2019.01.022>
- Critelli S., Criniti S. 2021. Sandstone petrology and provenance in fold thrust belt and foreland basin system. In: Al-Juboury A. (ed.). *Sedimentary Petrology: Implications in Petroleum Industry*. Croatia: IntechOpen, p. 1-15.
- Critelli S., Criniti S., Ingersoll R.V., Cavazza W. 2022. Temporal and spatial significance of volcanic particles in sand(stone): implications for provenance and palaeotectonic reconstructions. *Geological Society, Special Publications*, 520, 311-325. <https://doi.org/10.1144/SP520-2022-99>
- Critelli S., Ingersoll R.V. 1995. Interpretation of neovolcanic palaeovolcanic sand grains: an example from Miocene deep-marine sandstone of the Topanga Group (Southern California). *Sedimentology*, 42(5):783-804. <https://doi.org/10.1111/j.1365-3091.1995.tb00409.x>
- Cullers R.L., Barrett T., Carlson R., Robinson B. 1987. Rare-earth element and mineralogic changes in Holocene soil and stream sediment: a case study in the Wet Mountains, Colorado, U.S.A. *Chemical Geology*, 63(3-4):275-297. [https://doi.org/10.1016/0009-2541\(87\)90167-7](https://doi.org/10.1016/0009-2541(87)90167-7)
- Dani A.P.O., Remus M.V.D., Dani N., Lima E.F. 2017. Magmatismo basáltico do Andar Alagoas (Bacia de Campos). *Geologia USP. Série Científica*, 17(2):269-287. <https://doi.org/10.11606/issn.2316-9095.v17-373>
- Dias J.L., Oliveira J.Q., Vieira J.C. 1988. Sedimentological and Stratigraphic Analysis of the Lagoa Feia Formation, Rift Phase of the Campos Basin, Offshore Brazil. *Revista Brasileira de Geociências*, 18(3):252-260.
- Di Capua A., De Rosa R., Kereszturi G., Le Pera E., Rosi M., Watt S.F.L. 2022. Volcanically derived deposits and sequences: a unified terminological scheme for application in modern and ancient environments. *Geological Society, Special Publications*, 520, 11-27. <https://doi.org/10.1144/SP520-2021-201>

- Di Capua A., Groppelli, G. 2018. The riddle of volcanoclastic sedimentation in ancient deep-water basins: A discussion. *Sedimentary Geology*, **378**:52-60. <https://doi.org/10.1016/j.sedgeo.2018.05.008>
- Dickinson W.R. 1985. Interpreting provenance relations from detrital modes of sandstones. In: Zuffa G.G. (ed.). *Provenance of Arenites*. NATO-ASI Series, 148, p. 333-361.
- Doyle L.J. 2017. Continental margin. *Encyclopedia Britannica*. Available at: <https://www.britannica.com/science/continental-margin>. Accessed on: 10 Sept. 2022.
- Faure G. 1986. *Principles of isotope geology*. New York: John Wiley and Sons, 608 p.
- Fetter M., Deros L.F., Bruhn C.H.L. 2009. Petrographic and seismic evidence for depositional setting of giant turbidite reservoirs and the paleogeographic evolution of Campos Basin, offshore Brazil. *Marine and Petroleum Geology*, **26**(6):824-853. <https://doi.org/10.1016/j.marpetgeo.2008.07.008>
- Fisher R.V. 1961. Proposed classification of volcanoclastic sediments and rocks. *Geological Society of America Bulletin*, **72**(9):1409-1414. [https://doi.org/10.1130/0016-7606\(1961\)72\[1409:PCOVSA\]2.0.CO;2](https://doi.org/10.1130/0016-7606(1961)72[1409:PCOVSA]2.0.CO;2)
- Fleet A.J. 1984. Aqueous and sedimentary geochemistry of the rare earth elements. In: Henderson P. (ed.). *Rare earth element geochemistry*. Netherlands: Elsevier, v. 2, p. 343-373.
- Fodor R.V., Vetter S.K. 1984. Rift-zone magmatism: Petrology of basaltic rocks transitional from CFB to MORB, southeastern Brazil margin. *Contributions to Mineralogy and Petrology*, **88**(4):307-321. <https://doi.org/10.1007/BF00376755>
- Garzanti E., Doglioni C., Vezzoli G., Andò S. 2007. Orogenic belts and orogenic sediment provenances. *Journal of Geology*, **115**(3):315-334. <https://doi.org/10.1086/512755>
- Gill J.B., Bongiolo E.M., Miyazaki T., Hamelin C., Jutzeler M., Debari S. 2018. Tuffaceous mud is a volumetrically important volcanoclastic facies of submarine arc volcanism and record of climate change. *Geochemistry, Geophysics, Geosystems*, **19**(4):1217-1243. <https://doi.org/10.1002/2017GC007300>
- Graham I.J., Glasby G.P., Chuchman G.J. 1997. Provenance of the detrital component of deep-sea sediments from the SW Pacific Ocean based on mineralogy, geochemistry and Sr isotopic composition. *Marine Geology*, **140**(1-2):75-96. [https://doi.org/10.1016/S0025-3227\(97\)00006-6](https://doi.org/10.1016/S0025-3227(97)00006-6)
- Guardado L.R., Gamboa L.A.P., Lucchesi C.F. 1989. Petroleum geology of Campos Basin, Brazil: a model for producing Atlantic type basin. In: Edwards J.D., Santagrossi P.A. (eds.). *Divergent/Passive Margins Basins*. AAPG Memoir, p. 3-36.
- Hasenaka T., Carmichael I.S.E. 1985. A compilation of location, size, and geomorphological parameters of volcanoes of the Michoacan-Guanajuato volcanic field, central Mexico. *Geofísica Internacional*, **24**(4):577-607. <https://doi.org/10.22201/igeof.00167169p.1985.24.4.2179>
- Heilbron M., Silva L.G., Tupinambá M., Peixoto C., Lobato M., Rodrigues S., Ragatki C.D., Silva M.A., Monteiro T.L.V., Freitas N.C., Miguens D., Girao R. 2020. Proterozoic to Ordovician geology and tectonic evolution of Rio de Janeiro State, SE-Brazil: insights on the central Ribeira Orogen from the new 1:400,000 scale geologic map. *Brazilian Journal of Geology*, **50**(2):e20190099. <https://doi.org/10.1590/2317-4889202020190099>
- Inbar M., Hubp J.L., Ruiz L.V. 1994. The geomorphological evolution of the Paricutin cone and lava flows, Mexico, 1943-1990. *Geomorphology*, **9**(1):57-76. [https://doi.org/10.1016/0169-555X\(94\)90031-0](https://doi.org/10.1016/0169-555X(94)90031-0)
- Ingersoll R.V. 1990. Actualistic sandstone petrofacies: discriminating modern and ancient source rocks. *Geology*, **18**(8):733-736. [https://doi.org/10.1130/0091-7613\(1990\)018%3C0733:ASPDMA%3E2.3.CO;2](https://doi.org/10.1130/0091-7613(1990)018%3C0733:ASPDMA%3E2.3.CO;2)
- Kereszturi G., Németh K. 2012. Monogenetic Basaltic Volcanoes: Genetic Classification, Growth, Geomorphology and Degradation. In: Németh K. (ed.). *Updates in Volcanology: New Advances in Understanding Volcanic Systems*. Croatia: IntechOpen, p. 3-88.
- Le Maitre R.W., Streckeisen A., Zanettin B., Le Bas M., Bonin B., Bateman P. 2002. *Igneous Rocks: A Classification and Glossary of Terms: Recommendations of the International Union of Geological Sciences Subcommission on the Systematics of Igneous Rocks*. Edinburgh: Cambridge University Press, 236 p.
- Louback V.S., Valente S., Neys C., Ross J., Borghi L. 2021. Petrogenesis and geodynamics of Eocene alkaline intrusions in the pre-salt sedimentary sequence of Santos Basin, Brazil. *Lithos*, **400-401**:106400. <https://doi.org/10.1016/j.lithos.2021.106400>
- Manville V., Németh K., Kano K. 2009. Source to sink: a review of three decades of progress in the understanding of volcanoclastic processes, deposits, and hazards. *Sedimentary Geology*, **220**(3-4):136-161. <https://doi.org/10.1016/j.sedgeo.2009.04.022>
- Marcondes L.S. 2010. *Mapeamento Sísmico 3D das rochas vulcânicas Terciárias da região do Alto de Cabo Frio - Bacia de Campos - RJ*. Trabalho de conclusão de curso (Bacharelado em Geofísica), Instituto de Geociências, Universidade Federal Fluminense, Niterói, 48 p.
- Matos R.M.D. 2021. Magmatism and hotspot trails during and after continental break-up in the South Atlantic. *Marine and Petroleum Geology*, **129**, 105577. <https://doi.org/10.1016/j.marpetgeo.2021.105577>
- McDonough W.F., Sun S.S. 1995. The composition of the Earth. *Chemical Geology*, **120**(3-4):223-253. [https://doi.org/10.1016/0009-2541\(94\)00140-4](https://doi.org/10.1016/0009-2541(94)00140-4)
- McLennan S.M. 1989. Rare earth elements in sedimentary rocks: influence of provenance and sedimentary processes. In: Lipin B.R., Mckay G.A. (eds.). *Geochemistry and mineralogy of rare earth elements. Reviews in Mineralogy*, v. 21, p. 169-200.
- McPhie J., Doyle M., Allen R. 1993. *Volcanic Textures: a guide to the interpretation of textures in volcanic rocks*. Tasmania: Centre for Ore Deposit and Exploration Studies University of Tasmania, 196 p.
- Mello M.R., Rostirolla S.P., Peres W., Pedrosa O.A., Carvalho M.D., Cardoso Netto A. 2021. Tupi Field: The Largest Oil Producer in the South Atlantic Realm, Santos Basin, Brazil. In: Mello M.R., Pinar O.Y., Katz B.J. (eds.). *The Supergiant Lower Cretaceous Pre-Salt Petroleum Systems of the Santos Basin, Brazil*. USA: AAPG Memoir, v. 124, p. 395-430.
- Mizusaki A.M.P., Mohriak W.U. 1993. Sequências vulcano-sedimentares na região da Plataforma Continental de Cabo Frio. In: Simpósio de Geologia do Sudeste, Rio de Janeiro. *Atas...* p. 52-56.
- Mizusaki A.M.P., Petrini R., Bellieni G., Comin-Chiaromonte P., Dias J., De Min A., Picirillo E.M. 1992. Basalt magmatism along the passive continental margin of SE Brazil (Campos basin). *Contributions to Mineralogy and Petrology*, **111**:143-160. <https://doi.org/10.1007/BF00348948>
- Mohriak W.U. 2003. Bacias Sedimentares da Margem Continental Brasileira. In: Bizzi L.A., Schobbenhaus C., Vidotti R.M., Gonçalves J.H. (eds.). *Geologia, Tectônica e Recursos Minerais do Brasil*. Brasília: CPRM, p. 87-165.
- Mohriak W.U. 2020. Genesis and evolution of the South Atlantic volcanic islands offshore Brazil. *Geo-Marine Letters*, **40**(1):1-33. <https://doi.org/10.1007/s00367-019-00631-w>
- Mohriak W.U., Almeida J.C.H., Gordon A.C. 2022. South Atlantic Ocean: postbreakup configuration and Cenozoic magmatism. In: Santos A.C., Hackspacher P.C. (eds.). *Meso-Cenozoic Brazilian Offshore Magmatism: Geochemistry, Petrology and Tectonics*. London: Academic Press, p. 1-45.
- Mohriak W.U., Fainstein R. 2012. Phanerozoic regional geology of the Eastern Brazilian margin. In: Roberts D.G., Bally A.W. (eds.). *Regional Geology and Tectonics: Phanerozoic Passive Margins, Cratonic Basins and Global Tectonic Maps*. Waltham: Elsevier B.V., v. 7, p. 223-282.
- Mohriak W.U., Gordon A., Mello M.R. 2021. Origin and Petroleum System of the Cabo Frio High Between the Santos and Campos Basins: Reviewed Integration of Structural and Paleogeographic Reconstruction with the Oil and Gas Systems In: Mello M.R., Pinar O.Y., Katz B.J. (eds.). *The Supergiant Lower Cretaceous Pre-Salt Petroleum Systems of the Santos Basin, Brazil*. USA: AAPG Memoir, v. 124, p. 273-324.
- Moreira J.L.P., Esteves C.A., Rodrigues J.J.G., Vasconcelos C.S. 2006. Magmatismo, sedimentação e estratigrafia da porção norte da Bacia de Santos. *Boletim de Geociências da Petrobras*, **14**(1):161-170.
- Moreira J.L.P., Madeira C.V., Gil J.A., Machado M.A.P. 2007. Bacia de Santos. *Boletim de Geociências da Petrobras*, **15**:531-549.
- Németh K. 2010. Monogenetic volcanic fields: Origin, sedimentary record, and relationship with polygenetic volcanism. In: Cañón-Tapia E., Szakács A. (eds.). *What Is a Volcano?* USA: Geological Society of America, v. 470, p. 43-66.
- Nesbitt H.W. 1979. Mobility and fractionation of rare earth elements during weathering of a granodiorite. *Nature*, **279**:206-210. <https://doi.org/10.1038/279206a0>
- Nesbitt H.W., Macrae N.D., Kronberg B.I. 1990. Amazon deep-sea fan muds: light REE enriched products of extreme chemical weathering. *Earth and Planetary Science Letters*, **100**(1-3):118-123. [https://doi.org/10.1016/0012-821X\(90\)90180-6](https://doi.org/10.1016/0012-821X(90)90180-6)

- Oreiro S.G. 2006. Magmatismo e sedimentação em uma área na Plataforma Continental de Cabo Frio, Rio de Janeiro, Brasil, no intervalo Cretáceo Superior - Terciário. *Boletim de Geociências da Petrobras*, **14**:95-112.
- Oreiro S.G., Cupertino J.A., Sztamari P., Thomaz Filho A. 2008. Influence of pre-salt alignments in post-Aptian magmatism in the Cabo Frio High and its surroundings, Santos and Campos basins, SE Brazil: An example of non-plume-related magmatism. *Journal of South American Earth Sciences*, **25**(1):116-131. <https://doi.org/10.1016/j.jsames.2007.08.006>
- Pandolpho B.R., Klein A.H.F., Dutra I., Mahiques M.M., Viana A.R., Bueno G.V., Machado A.A., Camargo Y.L., Hercos C.M., Lima Y., Filho F.H.F., Theodoro C.E. 2021. Seismic record of a cyclic turbidite-contourite system in the Northern Campos Basin, SE Brazil. *Marine Geology*, **434**, 106422. <https://doi.org/10.1016/j.margeo.2021.106422>
- Pearce J.A. 1996. A user's guide to basalt discrimination diagrams. In: Wyman D.A. (ed.). *Trace element geochemistry of volcanic rocks: applications for massive sulphide exploration*. Canada: Geological Association of Canada, v. 12, p. 79-113.
- Rancan C.C., Oliveira L.C., Carmo I., Marins G.M., Pessoa V.C., Andrade H., Penatti A.P.R., Borges T.A., Silva R.C.B., Carlotto M.A., Bassetto M., Zanatta A.S. 2018. Rochas ígneas do Bloco de Libra, Bacia de Santos. In: Simpósio de Vulcanismo e Ambientes Associados, 7., 2018, Rio de Janeiro. Anais do 49º Congresso Brasileiro de Geologia, 7327.
- Rangel H.D. 2006. Manifestações magmáticas na parte sul da Bacia de Campos (Área de Cabo Frio) e na Bacia de Jequitinhonha. *Boletim de Geociências da Petrobras*, **14**(1):155-160.
- Ren K., Oliveira M.J.R., Zhao J., Zhao J., Oliveira L.C., Rancan C.C., Oliveira I.C., Deng Q. 2019. Using Wireline Logging and Thin Sections to Identify Igneous Contact Metamorphism and Hydrothermal Influence on Presalt Limestone Reservoirs in Libra Block, Santos Basin. In: Offshore Technology Conference Brasil. Anais... OTC-29818-MS.
- Rider M. 1996. *The geological interpretation of well logs*. United Kingdom: Rider-French Consulting, 280 p.
- Schattner U., Mahiques M.M. 2020. Post-rift regional volcanism in southern Santos Basin and the uplift of the adjacent South American coastal range. *Journal of South American Earth Sciences*, **104**, 102855. <https://doi.org/10.1016/j.jsames.2020.102855>
- Schön J.H. 2015. *Physical Properties of Rocks: Fundamentals and Principles of Petrophysics*. Waltham: Elsevier, 456 p.
- Sohn C., Sohn Y.K. 2019. Distinguish between primary and secondary volcanoclastic deposits. *Scientific Reports*, **9**, 12425. <https://doi.org/10.1038/s41598-019-48933-4>
- Sun S.S. 1980. Lead Isotopic Study of Young Volcanic Rocks from Mid-Ocean Ridges, Ocean Islands and Island Arcs. *Royal Society*, **297**(1431):409-445. <https://doi.org/10.1098/rsta.1980.0224>
- Sun S.S., McDonough W.F. 1989. Chemical and isotopic systematics of oceanic basalts: implications for mantle composition and processes. *Geological Society*, **42**:313-345. <https://doi.org/10.1144/GSL.SP.1989.042.01.19>
- Taylor S.R., McLennan S.M. 1985. *The continental crust: its composition and evolution*. Oxford: Blackwell, 328 p.
- Valloni R. 1985. Reading provenance from modern marine sands. In: Zuffa G.G. (ed.). *Provenance of Arenites*. NATO-ASI Series, v. 148, p. 309-332.
- Weaver B.L., Tarney J. 1981. Lewisian geochemistry and Archean crustal development models. *Earth and Planetary Science Letters*, **55**(1):171-180. [https://doi.org/10.1016/0012-821X\(81\)90096-0](https://doi.org/10.1016/0012-821X(81)90096-0)
- White J.D.L., Houghton B.F. 2006. Primary volcanoclastic rocks. *Geology*, **34**(8):677-680. <https://doi.org/10.1130/G22346.1>
- Winchester J.A., Floyd P.A. 1976. Geochemical magma type discrimination: application to altered and metamorphosed basic igneous rocks. *Earth and Planetary Science Letters*, **28**(3):459-469. [https://doi.org/10.1016/0012-821X\(76\)90207-7](https://doi.org/10.1016/0012-821X(76)90207-7)
- Winchester J.A., Floyd P.A. 1977. Geochemical discrimination of different magma series and their differentiation products using immobile elements. *Chemical Geology*, **20**:325-343. [https://doi.org/10.1016/0009-2541\(77\)90057-2](https://doi.org/10.1016/0009-2541(77)90057-2)
- Winter W.R., Jahnert R.J., França A.B. 2007. Bacia de Campos. *Boletim de Geociências da Petrobras*, **15**:511-529.
- Zou C., Zhang G., Zhu R., Yuan X., Zhao X., Hou L., Wen B., Wu X. 2013. *Volcanic Reservoirs in Petroleum Exploration*. Waltham: Elsevier, 204 p.
- Zuffa G.G. 1987. Unravelling hinterland and offshore paleogeography from deepwater arenites. In: Leggett J.K., Zuffa G.G. (eds.). *Marine Clastic Sedimentology: Concepts and Case Studies*. London: Graham and Trotman, p. 39-61.